Nitric Acid Particles in Cold Thick Ice Clouds Observed at Global Scale: Link with Lightning, Temperature, and Upper Tropospheric Water Vapor

H. Chepfer[1], P. Minnis[2], P. Dubuisson[3], M. Chiriaco[1], S. Sun-Mack[4], E. D. Rivière[5]

[1]LMD/IPSL, Université Pierre et Marie Curie, France

[2]NASA Langley Research Center, Hampton, VA, USA

[3]ELICO, Université du Littoral, France

[4]SAIC, Hampton, VA, USA

[5] LPCE, CNRS/Université d'Orléans, France

Submitted to Science

June 2005

Abstract

Signatures of nitric acid particles (NAP) in cold thick ice clouds have been derived from satellite observations. Most NAP are detected in the Tropics (9 to 20% of clouds with T< 202.5 K). Higher occurrences were found in the rare mid-latitudes very cold clouds. NAP occurrence increases as cloud temperature decreases and NAP are more numerous in January than July. Comparisons of NAP and lightning distributions show that lightning is the main source of the NO_x, which forms NAP in cold clouds. Qualitative comparisons of NAP with upper tropospheric humidity distributions suggest that NAP play a role in the dehydration of the upper troposphere when the tropopause is colder than 195K.

1. Introduction

Water vapor, the main atmospheric greenhouse gas (1), plays key role in climate change, especially when its effects in the upper troposphere are considered (2, 3). Mean upper tropospheric humidity (UTH) has been anomalously decreasing over the entire Tropics since 2001 (4). Dehydration of the upper troposphere (UT) over large areas in the Tropics is linked to variations in the temperature of the tropical tropopause layer (TTL), particularly in the winter hemisphere (5,6), but the processes inducing the variations in UTH are not well understood. Ice clouds (7,8) are involved in the UT dehydration (9,10) serving as both sinks and sources of humidity. However, the factors governing the relative amounts of UT frozen and gaseous water are poorly understood. Recently, condensed phase HNO_3 particles were measured in situ within ice clouds at temperatures *T* between 197 and 224 K (11) confirming the presence of nitric acid particles (NAP) near the tropical tropopause, a phenomenon that has been observed indirectly for some time (12-15). Other in situ (16) and model (17) studies demonstrated that UT nitric acid interacts with ice particles and modifies the UTH.

Satellite remote sensing is needed to better evaluate the role of HNO_3 in ice clouds and its impact on tropical UTH. Global distributions of NAP signatures in cold thick ice clouds derived from satellite data (18) are shown here for the first time. They are used to show that lightning is probably the main source of NO_x (HNO_3 precursor), and that NAP occurs more frequently at extremely low temperatures, suggesting that NAP could be involved in the UT dehydration anomaly associated with very low TTL temperatures.

2. Observations

2.1. Spatial distribution of NAP signatures

In terms of sheer numbers, NAP signatures are more common in clouds over ocean than those over land and they are seasonally (January/July) invariant: More than 40 and 21% of NAP occurs during night and day, respectively, over ocean (Table 1A). Over land, the daytime contribution in January is nearly twice that in July.

The distributions of NAP for cold clouds (Figure 1) correspond to the main convective areas and to a few areas off the Antarctic coast during July (not shown) that are likely associated with polar stratospheric clouds (19). The relative occurrence of NAP for T_{11} < 202.5 K is relatively constant at about 17-20% around the ITCZ over land and ocean during both months (Figures 2(a-b)). Moreover there is a persistent asymmetry between the two hemispheres above ocean, with a larger NAP frequency peak in the northern mid-latitudes. The maxima, located around 40° north and south of the ITCZ, reach values between 60 and 100%. Although the extremely cold clouds are less frequent in the mid-latitudes (Fig.S1a-b), when they occur there, they are more often associated (30 to 80%) with NAPs than when they occur in the Tropics.

NAPs in warmer clouds (T_{11} < 230 K) follow a pattern similar to those in cold clouds but are less frequent overall (Fig.2.c-d). NAP occur in the ITCZ area in only 5% of the tropical ice clouds indicating that their occurrence frequency mainly depends on cloud temperature. Relative maxima for those warmer ice clouds occur in January at 30°N over ocean at night, 30°S (Argentina/Africa) during the day, and 75°N (Greenland/Siberia) during the night. Those features are confirmed in the global means (Table 1C and (20)). For a constant cloud amount, the production of NAP is greater above ocean during the night than during the day and than above land at any time.

2.2. Time variation

Diurnal cycle: The NAP occurrence frequency varies as a function of local time (LT) in a similar fashion at all latitudes over a range of temperatures (Fig. 2e). The diurnal cycle amplitude decreases with increasing temperature, further supporting the idea that NAP is more common at lower temperatures. During daytime (1030 and 1330 LT), NAP occur more frequently above land than over ocean at all cloud temperatures, possibly as a result of stronger convection over land (21). The opposite occurs at 0130 LT when convection is reduced over most land areas. Over water, NAP signatures are more common at night than during the day, on average (Fig.2e, Table 1C). Conversely, there is no clear mean diurnal cycle over land (Fig.2e, Table 1C) despite some sharp day/night contrasts in specific regions such as the southern mid-latitudes (Fig. 2a-d).

Monthly variation: NAP occur more often in January than in July (Table 1A and 1B). Considering all ice clouds with $T_{11} < 230$ K, the NAP frequency is 17.6% higher in January than in July (Table1B). This increase is mainly due to NAPs associated with T_{11} between 220 and 230 K occurring over Greenland and Siberia (70°N, Fig.2d) during the winter night. These polar signatures are likely produced by NAP contained in PSCs located above very cold surfaces (19). Considering clouds with $T_{11} < 202.5$ K (tropical clouds, Fig.S1b), the global NAP occurrence increases by 7% between July and January (Table 1A). This rise is partly due to more frequent NAPs over land during the day along the ITCZ near Brazil and south central Africa (Fig. 1). Since the percentage of NAP occurrence is the same for both months (Table 1), this increase is mainly induced by more cold clouds in those regions (Fig.S1e) because of convection. The equivalent amount of cold clouds is not evident over Northern hemisphere land surfaces in July.

2.3. Temperature dependency.

The distributions in Fig. 1 are typical of other T_{11} and NAP ranges where the proportion of NAPs increases at lower temperatures. Figures 2f and S3a confirm that NAP frequency decreases with increasing cloud temperature with a maximum of 32% (25% see (20)) for $T_{11} < 195$ K. The slope of this variation is nearly the same for all cases, but increases for $T_{11} < 195$K. For clouds with $T_{11} < 210$ K and for constant values of T_{11}, NAP are less frequent in January than in July at all times of day over all surfaces (Fig.2f) independent of the cloud amount. Despite a consistent increase of NAP occurrence as temperature decreases, the frequency can vary by a factor of two at a constant temperature depending on the time of day (Figure S3a).

3. Discussion

Two different categories of ice clouds containing NAP are evident in the results: very cold ice clouds ($T_{11} < 202.5$K) resulting from convection around the ITCZ, and mid-latitude or polar (PSCs) ice clouds that can have higher temperatures ($202.5 < T_{11} < 230$K) but more frequently (30 to 70%) produce NAP than the tropical clouds. Of the ITCZ clouds, nearly 20% (or 9% Table 1C) contain nearly-constant signatures of NAP.

NAP such as Nitric Acid Trihydrate (NAT, 22-24) or NAT-like (16) particles are composed of HNO_3 and H_2O ($HNO_3.3H_2O$). Possible links between spatio-temporal distributions of NAP signatures and HNO_3 precursors as well as UTH are discussed hereafter.

3.1. Origin of HNO_3

HNO_3 occurs in significant amounts in the lower troposphere, but because of its high solubility it is scavenged by convective clouds, and can hardly be transported into the tropical UT. Hence HNO_3 occurring in the tropical UT is produced at high altitudes by oxidation of

NO_2 (NO_2 + OH+M -> HNO_3+M, M being a molecule of air). OH is formed during daytime as a result of photo-dissociation and can be consumed by oxidation reaction. NO_2 is naturally produced by lightning all over the globe and generated from anthropogenic sources like fossil fuel burning that produces NO_x (not soluble), which can be transported to the UT. The amount of HNO_3 available for formation of NAP in the tropical UT will result of a competition between two processes: an increased amount of HNO_3 precursor (NO_2) by lightning or anthropogenic sources and the scavenging of HNO_3 by convective clouds. Increased NAP occurrences (Fig.1) are not observed in cold ice clouds over fossil-fuel burning areas (e.g., eastern China coast, US, northern Europe), but NAP (Fig. 1) and lightning (Fig. 3) locations coincide over South America, sub-Saharan Africa, and Australia in January, and over the Sahel and Himalayas in July, as well as over the main marine convective areas. Those similarities suggest that lightning is the main source of NO_x in the production of HNO_3 and hence NAP. Because of typically stronger convection over land, lightning occurs more frequently over land than over oceans (25). The land-ocean contrast is very strong during the day with the 1600-LT lightning maximum (26) being nearly four times greater than over ocean. At other times though, the land-sea contrast is very small. Even though all satellite overpasses occur at times off this maximum lightning peak, NAP signatures present a land-ocean contrast during the day (Fig. 2e) that is consistent with lightning variation.

Ocean. In the $\pm$20° latitude belt, lightning occurs most often over the Tropical Western Pacific (TWP, Fig. 3) and Indian Oceans where there is a high frequency of NAP signatures (Fig.1).

Land. Most of the lightning regions included in the $\pm$20° latitude bands are consistent with the NAP signatures (Fig. 1 and 3). At 30°S, other important land regions with heavy lightning, such as Argentina, South Africa and southern Australia (Fig. 3) contribute little to NAP

occurrence in winter because the lightning is not associated with very cold clouds (Fig. S1b-d). Nevertheless, warmer clouds (230 K > T > 202.5 K) located in those regions can lead to a sharp NAP occurrence peak such as that at 30°S (Fig. 2d), which effectively corresponds to those active lightning areas. Similar correspondence appears in summer, as most of the lightning contribution occurs in the southern US where clouds with T_{11} < 202.5K occur less frequently. Those around 30°N (Fig. 2a) are associated with the Himalayas where both lightning and NAP signatures occur consistently. Direct comparison between NAP and lightning diurnal cycles averaged over the globe is not pertinent, because it is biased by cloud temperatures. Nevertheless, comparisons in specific lightning regions such as Brazil or sub-Saharan Africa in January reveal more NAP during the day (Fig.1) consistent with the lightning patterns.

3.2.*Link with UTH*

NAP (28) takes the form of NAT at very low temperatures (typically T<195K) and Δ-ice particles also called NAT-like particles (HNO_3 adsorbed on ice crystal surface) at higher temperatures (224>T>195K). In both temperature regimes, a change in UTH or an increase in NO_x concentration can alter the number of NAP particles, consequently pure NAT and Δ-ice particles interact with water vapor and could affect the UTH balance. Pure NAT particles will consume water vapor but formation of Δ-ice particles could cause an enhancement of UTH (16).

Global maps of UTH [Figure 4 in (29), (30)], lightning (Fig. 3) and NAPs (Fig. 2) show evident correlation between the spatial distribution of these three variables in July, with maximum occurrence in the convective areas**.** UTH reaches a maximum at midnight over ocean and at 0300 LT over land, where the amplitude of the diurnal cycle is significantly larger (29). Consistently, NAP frequencies over ocean peak during the night (Fig.2e). Above

land, the spatial variation of UTH is well correlated with lightning and NAP, but the diurnal cycle is not. That is possibly due the fact that, the lightning maximum (1600LT) is followed by the maximum deep convective cloudiness (1900LT (29)) that scavenged HNO_3 before the maximum UTH occurs (0300LT (29)). This phenomenon does not occur above ocean because the maximum deep convective cloud occurs later, 0900 LT the following day (29).

For a constant cloud temperature, NAP occurrence is larger in July than January independent of the cloud amount and the surface type (Fig. 2f). This can be explained by the greater humidity available in July (6) to produce NAP.

3.3. Link with temperature.

Temperature plays a key role in the process because, for a given quantity of water vapor and HNO_3 in the UT, lower temperatures can lead to a slight decrease in UTH through the creation of NAT while warmer clouds can cause a slight increase in UTH through the creation of Δ-ice (16). The NAP occurrence clearly increases when temperature decreases (Fig. S3a) and shows a discontinuity at T < 195 K (the NAT formation temperature in tropical conditions). Over ocean, the amount of HNO_3 precursor is quite stable in time when considering lightning as the dominant source of NO_x (no strong lightning diurnal cycle above ocean (26), the amplitude of the UTH diurnal cycle is significantly less than over land (29), and the cloud amount (T_{11}<202.5K) is nearly constant. Hence, a change in the TTL temperature can directly amplify or reduce the creation of NAT, and so reduce or increase the UTH.

On average, the mean frequency of NAP in cold ice clouds (T_{11} < 202.5 K) is higher in January than in July (+7%), which is consistent with the lower January TTL temperature, leading to more clouds with T_{11} < 195 K (Fig. S1e, S3b) and consequently to a higher contribution of those clouds to the total number of NAP signatures (Fig.2g). The other cold

clouds with $195 < T_{11} < 202.5$ K are less efficient in producing NAP (Fig.2f), but are more numerous (Fig. S3b) resulting in a significant contribution to the total number of occurrences (Fig. 2g). Their contribution to NAP formation is very strong in July when the UTH is higher. At those temperatures, NAP help maintain the relatively high UTH. For a constant temperature, more NAP is produced because more water vapor is available, but because NAP forms in Δ-ice particles at those temperatures, the UTH is enhanced (16) and, therefore, UTH remains higher in July. During January, because of the lower tropopause temperature, the clouds are colder, producing more NAP particles with a larger proportion of NAT (T_{11}<195K in Fig. 2g) that consume UTH and tend to dehydrate the UT. The possible role of these NAP processes in the UTH regulation is supported by the fact that most NAP signatures occur over ocean with large contributions over the TWP and Indian Ocean. Those regions have very cold TTL temperatures, typically 200-196K in July, with a significant seasonal variation leading to a cooling (195-190K) in January (5) that is correlated to an unexplained decrease in UTH. The high frequency of NAP observed in this region and the differences in the NAP formation processes occurring at the threshold of 195 K (Fig. S3a) indicate that creation of NAT particles in the ice cloud tops is a process involved in the dehydration anomaly. The same process could also help explain the global decrease in UTH associated with a TTL temperature anomaly (-2 to -3K) under progress since 2001 (6). For constant ice cloud ocean coverage and lightning occurrence, a drop in temperature by a few degrees makes the NAT creation process nearly twice as efficient when the barrier of 195 K is reached (Fig. S3a). The UTH enhancement due to Δ-ice particles, then, would not be sufficient to compensate the UTH consumed by the relatively dense NAT, which precipitate more quickly than ice particles of similar volume, and the UT would be dehydrated.

5. Conclusion

The January and July datasets indicate the presence of NAP in 20% (9%) of cold clouds (T_{11} < 202.5K) in the Tropics, and even more often in the mid-latitudes (30 to 80% for T_{11} <230K). A majority of NAP signatures occur above tropical oceans. Lightning is a major source of NO_x for formation of NAP in the upper troposphere. Comparison between NAP frequency, cloud temperature, and UTH indicate that two regimes of NAP formation co-exist. When T_{11} < 195 K, a large amount of NAT particles form and consume water vapor, but when T_{11} > 195 K, fewer NAT particles form while Δ-ice particles become more common and enhance the UTH. In January, the NAT are more frequent than in July because the ITCZ TTL is colder than 195 K, hence, more extremely cold clouds (T < 195 K) form, and the NAP particles take the form of NAT, dehydrating the upper troposphere. In July, the TTL temperature exceeds 195 K causing most of the NAP to take the form of Δ-ice particles that help maintain the upper troposphere humidity. This process could explain part of the dehydration anomaly observed in the TWP with the decrease in TTL temperature being the driving force. It could also be a process involved in the UT dehydration observed over 5 years (6). It is not possible from the current results to quantify the relative proportions and total impact of the two NAP formation processes in the upper troposphere dehydration: Are NAP particles the primary or an anecdotal process leading to upper tropical troposphere dehydration ?

Acknowledgments: The CERES MODIS analyses were supported by the NASA Earth Sciences Program through the CERES Project.

References.

1. D. Key, J. M. Russel, C. Philips, Eds, SPARC Assesment of Upper tropospheric and Stratospheric Water Vapour (World Climate Research Programme No113, World Meteorological Organisation/TD No 1043, SPARC Report No2, 2000)
2. Climate Change, 2001: The Scientific Basis (Intergovernmental Panel on Climate Change (IPCC), Cambridge Univ. Press, 2001)
3. D. L. Hartman, *Science*, **295**, 811 (2002).
4. W.J. Randal, F. Wu, S. J. Oltmans, K. Rosenlof, G. E. Nedoluha, *J. Atmos. Sc*, **61**, 2133 (2004).
5. J.R. Holton, A. Gettelman, *Geophys. Res. Lett*. **28**, 2799 (2001).
6. X. Zhou, M. A. Geller, M. Zhang, *J.of. Climate*, **17**, 2901 (2004).
7. Liou K.N*., Mon Wea. Rev*, **114,** 1167 (1986).
8. Stephens, G. L., S. C. Tsay, P. W. Stackhouse Jr., and P. J. Flateau, *J. Atmos. Sci.,* **47**, 1742 (1990)
9. D. L. Hartman, J. R. Holton, Q. Fu, *Geophys. Res. Let*., **28**, 1969 (2001).
10. A.E. Dessler and S.C. Sherwood, *Atmos. Phys. Chem. Phys. Discuss*., **3**, 44-89-4513 (2003).
11. Popp, P. J., R. S. Gao, T. P. Marcy, D. W. Fahey, P. K. Hudson, T. L. Thompson, B. Karcher, B. A. Ridley, A. J. Weinheimer, D. J. Knapp, D. D. Montzka, D. Baumgardner, T. J. Garrett, E. M. Weinstock, J. B. Smith, D. S. Sayres, J. V. Pittman, S. Dhaniyala, T. P. Bui, and M. J. Mahoney, *J. Geophys. Res.*, **109**, 10.1029/2003JD004255 (2005).
12. P. Hamill and G. Fiocco *Geophys. Res. Let.*, **15**, 1189, (1988).
13. Omar A. H. and C. S. Gardner, *J. Geophys. Res.*, **106**, 1227 (2001).
14. Hervig. M. and M. McHugh, *Geophys. Res. Lett.*, **29**, 101029/2001GL014271 (2002).
15. Jensen, E. and K. Drdla, *Geophys. Res. Lett*., **29**, 10.1029/2002GL015190 (2002).
16. Gao, R.-S., P. J. Popp, D. W. Fahey, T. P., Marcy R. L. Herman, E. M. Weinstock, D. G. Baumgardner, T. J., Garrett, K. H. Rosenlof, T. L. Thompson, P. T. Bui, B. A. Ridley, S. C. Wofsy, O. B. Toon, M. A. Tolbert, B. Kärcher, Th. Peter, P. K. Hudson, A. J. Weinheimer, and A. J. Heymsfield, *Science*, **303**, 516, (2004).
17. M. Kramer, C. Schiller, H. Ziereis, J. Ovarlez and H. Bunz, *Tellus*, (2005).
18. *Science Online Material:* (1) Method and dataset
19. C. Voigt et al., *Science*, **290**, 1756 (2000).
20. *Science Online Material:* (2) Uncertainty on NAP occurrence

21. M.A. LeMone, E.J. Zipser, J. Atmos. Sci., 37, 2444 (1980).
22. D.R. Hanson, K. Mauersberger, *Geophys. Res. Let.,* **15**, 855 (1988).
23. D. R. Wornsop, L. E. Fox, M. S. Zahniser, S. C. Wosfy, **Science**, 259, 71 (1993).
24. Toon O. W., M. A. Tolbert, B. G. Koehler, M. Middlebrook, and J. Jordan (1994), Infrared optical constants of H2O ice, amorphous nitric acid solutions, and nitric acid hydrates, *J. Geophys. Res.*, *99*, **25**,631-25,654.
25. D.J. Boccipio, S. Goodman, S. Heckman, *J. Appl. Meteo.,* **39**, 2231 (2000).
26. Williams E., K. Rothkin, and D. Stevenson, D. Boccippio, *J. Appl. Meteo.,* **39**, 2223 (2000).
27. B. J. Soden, *Geophys. Res. Lett.,* **27**, 2173 (2000).
28. Passive remote sensing can not distinguish between tenuous NAT cloud layer located slightly above (lower temperature) the convective cloud and Δ-ice particle located at warmer temperatures at the top of the convective cloud itself.
29. Tian B., B. J. Soden, and X. Wu, *J. Geophys. Res*., **109**, 10.1029/2003JD004117 (2004).
30. Global-scale UTH observations are available only from satellite data and correspond to a broad layer in the upper troposphere (200-500hPa) in cloud free areas (29 and 26). Thus, comparisons of UTH with NAP occurrences observed only in presence of high clouds can only be qualitative, at best.

Table 1:
A) **Distribution of the NAP signatures all over the globe** (except very high latitudes) for cloud brightness temperature at 11 μm (T_{11}) < 202.5K. NAP are detected in thick cold ice clouds using Negative Brightness Temperature Differences (NBTD) between the 11 and 12-μm radiances measured by *Moderate Resolution Imaging Spectro-radiometer* MODIS (18).
B) Same as A for T_{11}<230K.
C) Average percentage of NAP signatures in ice clouds all over the globe. Values given in () assume -0.2K bias on NBTD measured by MODIS (20).

	January	**July**
A. Distribution of NAP signatures (T_{11}<202.5K)		
Total Nb of NAP pixels	1548833	1448133 (-7%)
Ocean -Day	21%	22.5%
Land-Day	21% (strong increase South America)	13.5%
Ocean -Night	41%	45.5%
Land-Night	17%	20%
B. Distribution of NAP signatures (T_{11}<230K)		
Total Nb of NAP pixels	8013279	6812378 (-17.6%)
Ocean -Day	21%	23.5%
Land-Day	15%	18.5%
Ocean -Night	33%	42%
Land-Night	31% (strong increase Groenland/Siberia 220K<BT-11<230K)	16%
C. Average % of NAP signatures in clouds T_{11}<202.5K ,NBTD<0, (NBTD<-0.2)		
Ocean -Day	15% (6%)	16%
Land-Day	19% (8%)	20%
Ocean -Night	22% (10%)	23%
Land-Night	18% (8%)	21%

Figure 1: **NAP frequencies** in cloudy pixels with T_{11} between 202 and 202.5 K with NBTD between 0 and -0.5 K (18) from MODIS/*Aqua*.

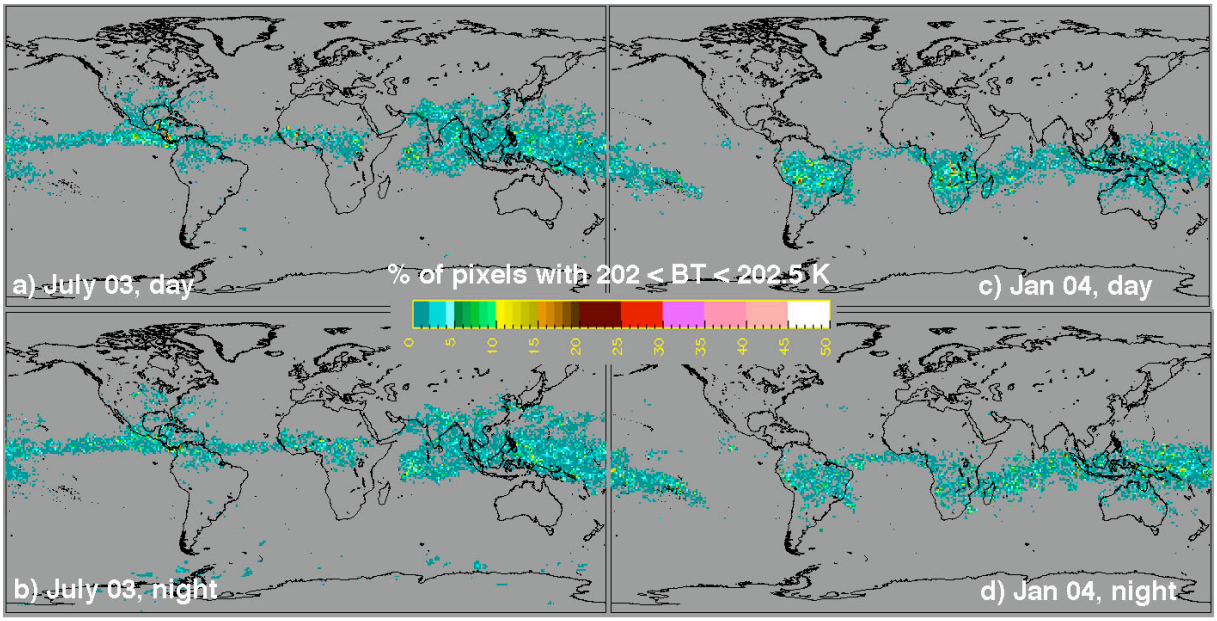

Figure 2:

(a-d) NAP frequencies as a function of latitude from MODIS/*Aqua*. For clouds with T_{11} <202.5K (a) July 2003 (b) January 2004. For clouds with T_{11} <230K (c) July 2003 (d) January 2004

(e) Diurnal cycle of NAP frequencies from MODIS/*Aqua* (1330 and 0130LT) and /*Terra* (1030 and 2230LT) for clouds with T_{11} <202.5K in January 2003. (NBTD<-0.2K, see (20))

(f) NAP frequencies as a function of T_{11} from MODIS/*Aqua* in July and January. In x-axis, classes 0 to 7 correspond to T_{11} (< 195K),(195-197.5),(197.5-200),(200-202.5),(202.5-205),(205-210),(210-220),(220-230)

(g) Distribution of the total NAP amount in cold clouds (T_{11}<202.5K) above land and ocean as a function of T_{11} in January and July from MODIS/*Aqua*.

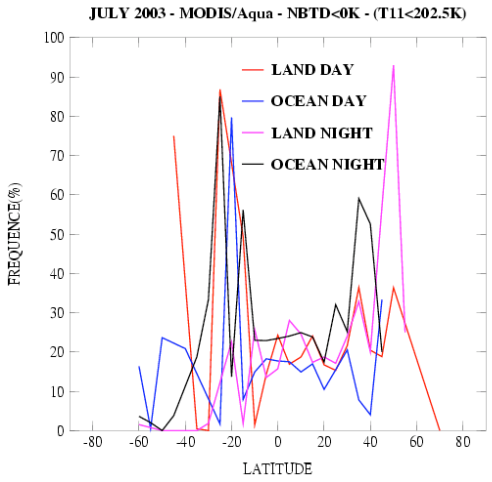

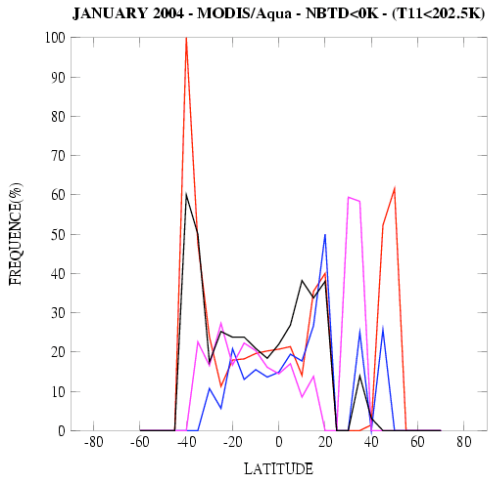

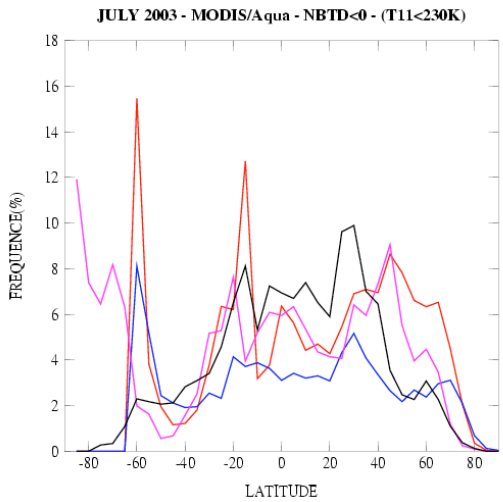

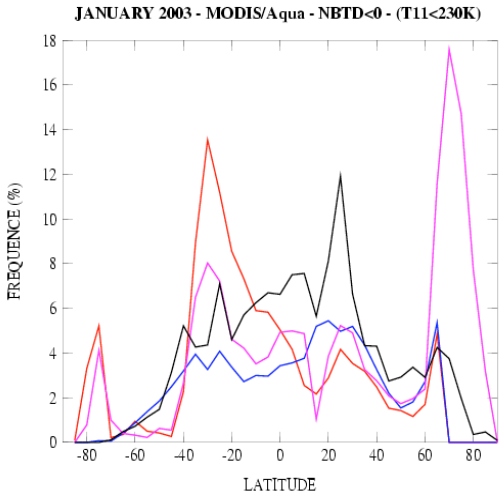

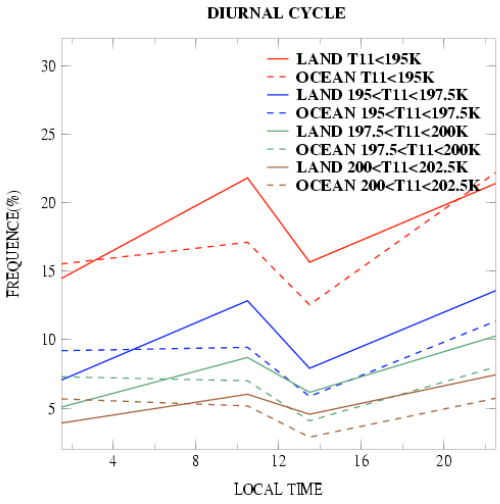
DIURNAL CYCLE
LAND T11<195K
OCEAN T11<195K
LAND 195<T11<197.5K
OCEAN 195<T11<197.5K
LAND 197.5<T11<200K
OCEAN 197.5<T11<200K
LAND 200<T11<202.5K
OCEAN 200<T11<202.5K
FREQUENCE(%)
LOCAL TIME

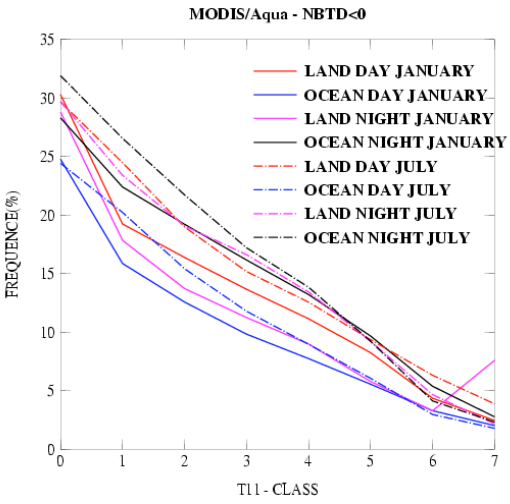
MODIS/Aqua - NBTD<0
LAND DAY JANUARY
OCEAN DAY JANUARY
LAND NIGHT JANUARY
OCEAN NIGHT JANUARY
LAND DAY JULY
OCEAN DAY JULY
LAND NIGHT JULY
OCEAN NIGHT JULY
FREQUENCE(%)
T11 - CLASS

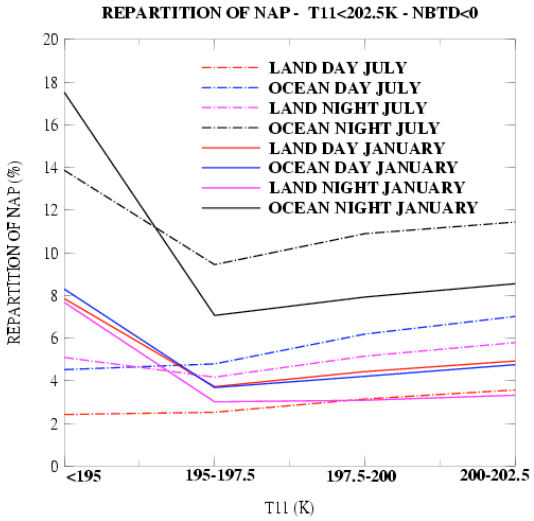
REPARTITION OF NAP - T11<202.5K - NBTD<0
LAND DAY JULY
OCEAN DAY JULY
LAND NIGHT JULY
OCEAN NIGHT JULY
LAND DAY JANUARY
OCEAN DAY JANUARY
LAND NIGHT JANUARY
OCEAN NIGHT JANUARY
REPARTITION OF NAP (%)
<195
195-197.5
197.5-200
200-202.5
T11 (K)

Figure 3: Lightning flashes measured by LIS onboard Tropical Rainfall Monitoring Measurements (TRMM) satellite during (a) summer 2003 and (b) winter 2004. TRMM precesses through all times of day over a 45-day period. The lightning flashes measured therefore, are diurnal averages including both high and low convective activity times. *Courtesy of NASA/MSFC*.

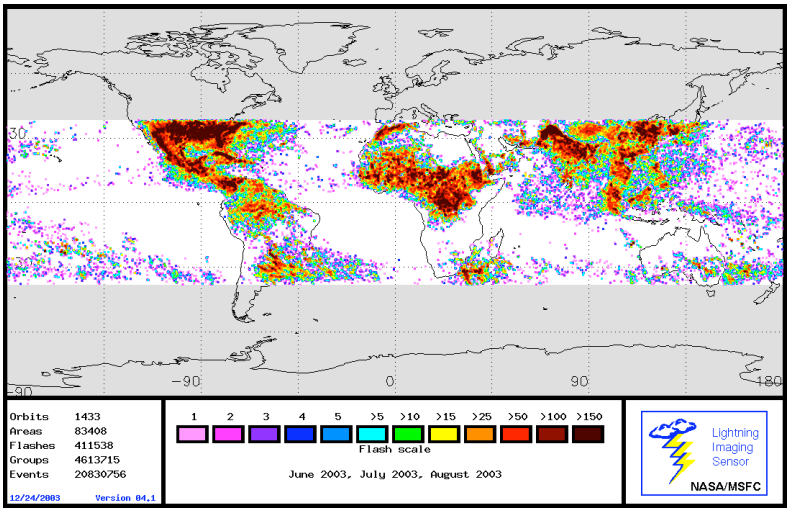

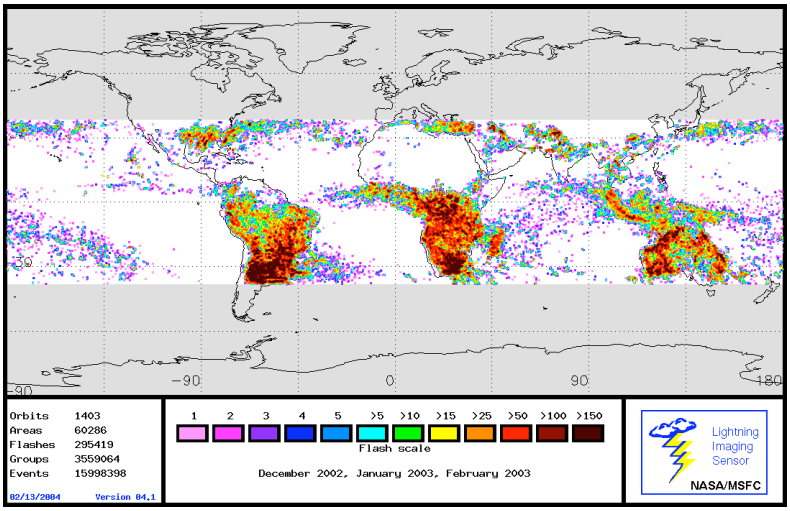

Supporting Material Online

(1) Method and dataset.

In an attempt to explain radiance anomalies associated with ice cloud retrievals, a remote sensing technique was developed to detect the signature of nitric acid in ice clouds from satellite observations (S1). Nitric acid is detected in thick cold ice clouds using brightness temperature differences (BTD) between the 11 and 12-μm radiances measured by satellite imagers. For pristine ice clouds and perfect satellite calibrations, the BTD will always be zero or positive because ice and water vapor are more absorptive at 12 than at 11 μm. Negative BTDs (NAPs) occur in the presence of nitric acid located in or above a thick cold ice cloud because HNO_3 has an 11-μm absorption band. The effect is only detectable when viewing a thick cold ice cloud, which acts as a blackbody that masks the upwelling radiances from under the cloud (S1). This signature does not occur for optically thin ice clouds because BTDs for optically thin cirrus clouds are positive and any nitric acid that is present in those clouds would only make the BTDs less positive. Furthermore, NBTD can also be observed in radiances from dust storms (S2-S3) as a result of the absorption characteristics of sand and volcanic ash aerosols. Selection of only thick high clouds precludes misidentification of aerosols as a nitric acid signal.

Moderate Resolution Imaging Spectroradiometer (MODIS, S4-6) data collected from *Terra* and *Aqua* in January 2003 as well as from *Aqua* in July 2004 are used to examine the global distributions of NBTD in ice clouds. Cloudy pixels are identified as in *(*S7*)* as part of the Clouds and the Earth's Radiant Energy System cloud products. The uncertainty in brightness temperature measured by MODIS is nominally less than 0.05 K.

Figures S1c-d show the number of cloud events with 11-μm brightness temperatures $T_{11} < 202.5$ K as a function of latitude, indicating that they occur mostly at low latitudes +30°

around the ITZC (Inter Tropical Convergence Zone) located at 10°N in July and 5°S in January, and also in small quantities in the mid-latitude winter hemisphere. There, the cloudy pixels may also be due to false cloud detection above snow surfaces, which are common at those latitudes in winter. There are naturally more cloud events occurring above sea surfaces than over land. No significant diurnal variation in frequency of occurrence is evident except during July above land, where more cold clouds occur at night than during the day. Cold clouds are slightly more numerous in January than during July. The only noticeable difference between the months is that the cold clouds over land are significantly greater in January at all latitudes during the daytime. At high latitudes in the winter hemisphere, the scarcity of potential measurements during daytime precludes the use of the data for defining a diurnal cycle. Hence, data corresponding to latitudes poleward of 60°N in January and 50°S in July are not considered in the following discussion.

The number of cloud events when $T_{11} < 230K$ (Fig. S1a-b) is large at nearly all latitudes. The event frequencies have quite similar characteristics in January and July with two relative minima in the summer hemisphere at a distance of 30° of latitude from the ITCZ in the winter hemisphere.

Very cold clouds with $T_{11} < 195K$ (Fig. S1e) occur relatively frequently around the ITCZ with more cold clouds during the night over ocean and more above ocean than over land surfaces. Very cold clouds are more abundant in January than in July as expected given the seasonal tropopause temperature variations along the ITCZ (5). The diurnal variations above ocean are similar during the two months, but different above land. Convection over Brazil and sub-Saharan Africa causes a significant increase in daytime clouds over land during January.

(2) Uncertainty in NAP occurrence

To account for possible measurement biases for $T_{11} < 230$ K, Figure S2 and Table 1C show the NAP distribution obtained in selecting NBTD<-0.2K instead of NBTD<0. This precaution to avoid overestimation of NAP signatures in ice clouds reduces the occurrence frequency by a factor of two. Typically 5 to 15% of clouds with $T_{11} < 202.5$K around the ITCZ have NBTD < -0.2 K (Fig. S2) and over ocean at night NBTD < -0.2 K in only 10% of cases compared to 22% for NBTD < 0.0 K (Table 1C). The frequency of the NAP signature is strongly variable with time during the day when the threshold is reduced (Fig. S3).

The low percentage of NAP in ice clouds associated with large brightness temperatures (Fig. S3) can be interpreted as an effective decrease of the condensed nitric acid concentration within the cloud or as a decrease of the cloud opacity, which leads to a smaller contrast between the two channels for the same condensed nitric acid concentration. It follows that the nitric acid condensates in ice clouds will be underestimated for non-opaque clouds, and the statistical results (Fig. 2 and S2) should be considered as possibly underestimating NAP frequencies.

References for Supporting On-line Material

S1. H. Chepfer, P. Dubuisson, M. Chiriaco, P. Minnis, S. Sun-Mack, E. Rivière*, J. Geophys. Res.*, submitted (2005)

S2. Gu, Y., W. I. Rose, and G. J. S. Bluth, *Geophys. Res. Lett.*, *30*, 10.1029/2003GL017405. (2003)Sokolik, I., *Geophys. Res. Lett.*, *29*, doi:10.1029/2002GL015910 (2002).

S3. King, M. D., W. P. Menzel, P. S. Grant, J. S. Myers, G. T. Arnold, S. E. Platnick, L. E. Gumley, S.-C. Tsay, C. C. Moeller, M. Fitzgerald, K. S. Brown, and F. G. Osterwisch, *J. Atmos. Oceanic Tech.*, *13*, 777 (1996).

S4. King, M. D., W. P. Menzel, Y. J. Kaufman, D. Tanre, B. C. Gao, S. Platnick, S. A. Ackerman, L. A. Remer, R. Pincus, and P. A. Hubanks, *IEEE Trans. Geosci. Remote Sens.*, *41*, 442, (2003).

S5. Platnick, S., M. D. King, S. A. Ackerman, W. P. Menzel, B. A. Baum, J. C. Riedi, and R. A. Frey, *IEEE Trans. Geosci. Remote Sens.,* 41, 459, (2003).

S6. Minnis et al., *Proc. SPIE 10th Intl. Symp Remote Sens., Conf. Remote Sens. Clouds and Atmos.*, Barcelona, Spain, September 8-12, 37-48. (2003)

Figure S1: Number of cloudy pixels as a function of latitude.
a-b) T_{11} <230K (solid line), T_{11} < 202.5K (dashed line), MODIS/*Aqua*, July/January
c-d) T_{11} <202.5K, July (*Aqua*), January (*Aqua* and *Terra*)
e) T_{11} <195K, *Aqua*, January/July

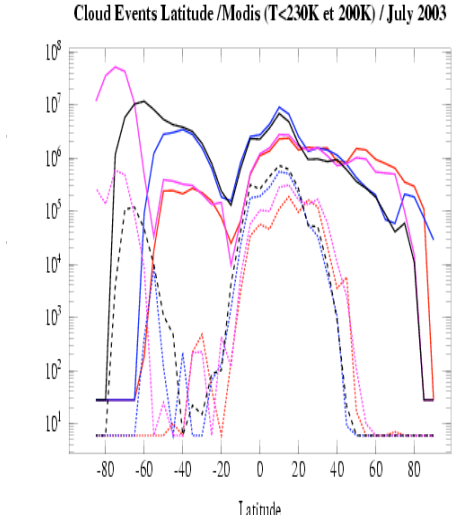

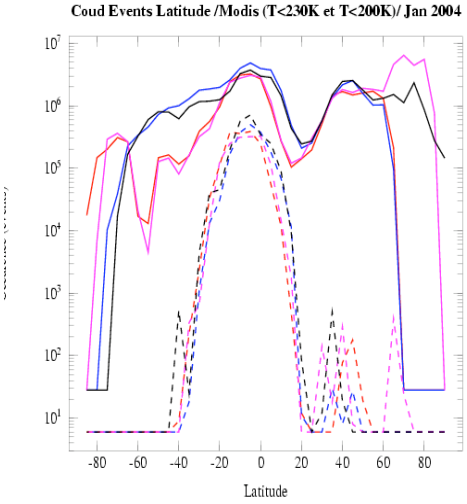

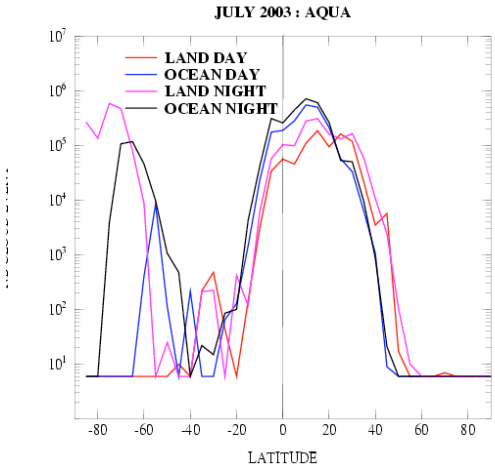

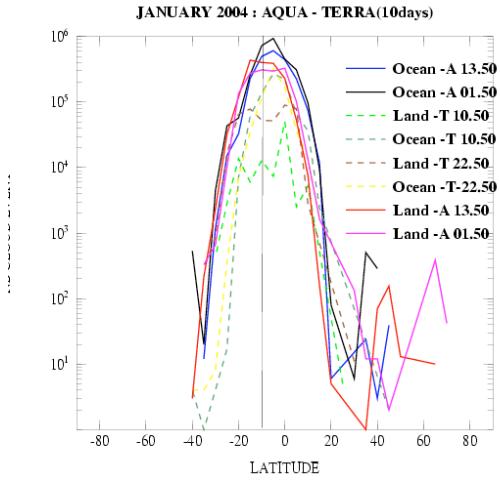

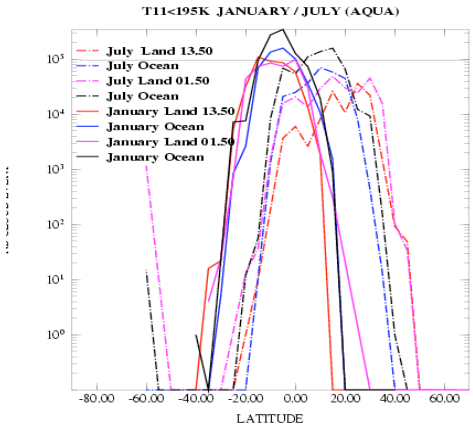

Figure S2: NAP frequencies as a function of latitude. Same as Fig. 1b but assuming a -0.2K bias on NBTD measured by MODIS (NBTD<-0.2K).

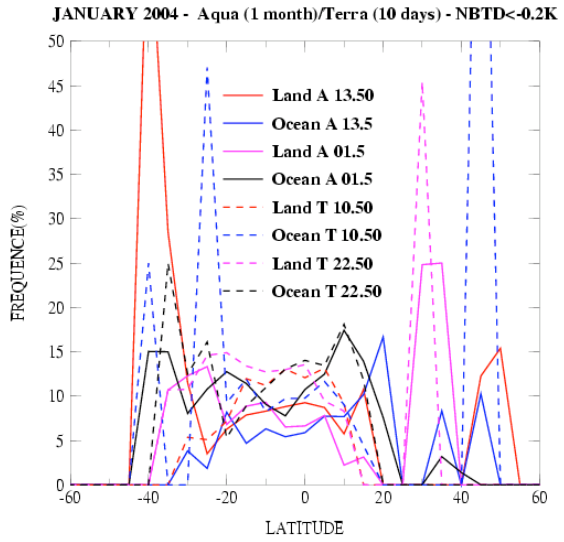

Figure S3:

(a) **NAP frequencies as a function of T_{11}**. Same as Fig.1f but for NBTD<-0.2K in January only including MODIS/*Aqua* and /*Terra* data.

(b) **Number of cloud events as a function of T_{11}** in January and July from MODIS/Aqua. January (solid line) and July (dashed line).